




Thermally stable and strong bulk Mg–MgO in situ nanocomposites by reactive cryomilling and high-pressure consolidation

Xuecheng Cai¹, Shengwei Xin¹, Baoru Sun¹, Hongwei Cui², Hui Yu³, Qiuming Peng¹, and Tongde Shen^{1,*} 

¹ State Key Laboratory of Metastable Materials Science and Technology, Yanshan University, Qinhuangdao 066004, People's Republic of China

² School of Materials Science and Engineering, Shangdong University of Technology, Zibo 255049, People's Republic of China

³ School of Materials Science and Engineering, Hebei University of Technology, Tianjin 300130, People's Republic of China

Received: 16 October 2017

Accepted: 15 January 2018

Published online:
22 January 2018

© Springer Science+Business Media, LLC, part of Springer Nature 2018

ABSTRACT

Nanoparticles have great potentials to improve the strength of metal matrix composites, but unfortunately, they tend to grow at high temperatures and are difficult to disperse uniformly with a high content, limiting the improvement in thermal stability and mechanical properties. Here we show the synthesis and performance of Mg–MgO in situ nanocomposites with a fraction of up to 40 vol% MgO nanoparticles. Our synthetic strategies include reactively cryomilling Mg with oxygen and subsequently consolidating the cryomilled powders under a high pressure of 6 GPa. Dispersed MgO nanoparticles with a fine particle size of 7.8 ± 1.7 nm are mainly situated at grain boundaries and exhibit a strong interfacial bonding with Mg matrix. Because of the strong Zener pinning effect of in situ formed MgO nanoparticles, the thermal stability is largely enhanced from ~ 100 °C for nanocrystalline Mg to 400 °C for Mg–10vol%MgO. The high thermal stability of Mg–MgO enables us to consolidate the cryomilled powders at a high temperature of 500 °C under a pressure of 6 GPa and achieve bulk Mg–MgO nanocomposites with a high compressive yield strength: 562 and 688 MPa for Mg–10vol%MgO and Mg–20vol%MgO, respectively. Meanwhile, the room-temperature hardness of the Mg–MgO nanocomposites increases linearly with the content of MgO nanoparticles and reaches 3.65 GPa for Mg–40vol%MgO. Furthermore, the MgO nanoparticles significantly improve the high-temperature hardness of nanocrystalline Mg.

Address correspondence to E-mail: tdshen@ysu.edu.cn

Introduction

Magnesium matrix composites are attractive structural materials for automotive and aerospace applications due to their increased hardness, strength, and even low-temperature superplasticity [1–5]. However, second-phase particles obtained by heat treatments tend to dissolve or grow at high temperatures, resulting in a loss of strengthening. Reinforcement of the ductile magnesium matrix with thermally stable and stiff ceramic particles such as oxides, nitrides, carbides provides a combination of superior properties of the metal matrix and the ceramic phases [5–8]. For most of the particle-reinforced metal matrix composites, however, the size of the ceramic particles is typically in the scale of micron meters. This leads to limited improvement in strength and significant reduction in ductility and toughness, which is mainly due to the easy initiation and propagation of cracks in the micrometer-sized particles and/or at the particle/matrix interfaces [2–4]. Nanoparticles have great potentials to improve the strength and maintain the plasticity of metals, but unfortunately, they are difficult to disperse uniformly with a high content, resulting in a saturation of strength or hardness and a degradation of plasticity [9–12]. Thus, reinforcing the metal matrix with a high content of uniformly dispersed nanoparticles plays an important role in producing high-performance metal matrix composites.

Different techniques, such as ingot metallurgy [13, 14], powder metallurgy [15, 16], rapid solidification [17], mechanical alloying [18–22], have been developed for the production of nanocrystalline Mg and Mg-based nanocomposites. Mechanical alloying (MA) is a simple and widely used processing route for the synthesis of nanocrystalline alloy and nanocomposite powders. A homogeneous distribution of nanosized reinforcing particles can be achieved by the MA process. In addition, prolongation of milling time can promote the formation of nanocrystalline matrix. Another advantage of MA is that both matrix and reinforcement are formed by in situ processes where chemical reactions and phase transformations take place because of the application of mechanical energy [21, 23–27]. Thus, MA has been widely used as a processing route for the synthesis of composites by in situ reactions. The in situ processes make composites a clean, contamination-free and well-bonded particle/matrix interface. This interface

is much stronger than that of mechanical interlocking and organic combination and thus leads to significantly enhanced mechanical and thermal properties [28–33]. As well known, however, Mg powders are so sticky to be refined and too difficult to be heavily cold-worked due to dynamical recovery during MA. Thus, a cryomilling technique has been used to suppress the dynamical recovery and to prepare new hydrogen-storage materials [34, 35], structural nanocrystalline alloys and nanocomposites [36–39]. It has been reported that the cryomilling technique alters the material properties and results in better refined structures in a shorter milling time, which is attributed to the relatively high strain rates, large cumulative strains and the suppression of the recovery process at cryogenic temperatures.

Once nanocomposite powders are prepared, how these powders can be consolidated into bulk and full-density compacts preserving the nanocrystalline structures should often be considered. This is especially important for mechanically alloyed nanocrystalline Mg powders because of their low thermal stability—grain growth occurs even at room temperature [40–42]—and more often than not, their abnormal grain growth (AGG). The low thermal stability provides an obstacle for using a high temperature to remove all porosities and obtain a good inter-particle bonding during consolidation since an intensive grain growth often occurs and degrades their mechanical properties. Thus, a high thermal stability is a prerequisite for the preparations and applications of nanocrystalline Mg alloys and Mg-based nanocomposites. There are two basic scientific strategies to hinder grain growth known as thermodynamic and kinetic stabilization, respectively. Thermodynamically, grain growth can be inhibited by the grain-boundary segregation of solute atoms [43–46]. The thermodynamic strategy has been exhaustively studied in many two-component alloy systems where the solute has a high tendency for segregation to grain boundaries (GBs) and in several ternary systems [47–49], where complex interactions can occur between constituent elements. Kinetically, second phase or solute drag can be used to slow down the migration of GBs. The kinetic strategy with a good flexibility has been extensively studied in many alloy systems [27, 42, 50–52]. The critical point for the kinetic stabilization strategy is to obtain a microstructure with a high content of fine and thermally stable particles uniformly distributed in the

matrix. This will increase the pinning pressure exerted by the particles on grain boundary (GB) and thus impede GB mobility, resulting in a high thermal stability. In addition, thermally stable nanoparticles with a strong interfacial bonding with the matrix can effectively improve the mechanical properties at elevated temperatures [5, 6, 53]. The nanoparticles residing at GBs can pin the GBs, improving the stability of the nanograins by increasing the energy barrier for grain-boundary activities such as grain-boundary sliding under elevated-temperature conditions.

Besides the above two intrinsic factors that may inhibit grain growth, a promising high-pressure consolidation method allowing to retain the nanocrystalline structures can also be considered. It is worthwhile to note that limited grain growth occurs after applying a high pressure to the order of magnitude of GPa to consolidate nanocrystalline FeAl intermetallic and some nanocomposites [54–56]. In general, the diffusion coefficient decreases with pressure [57]. Thus, the inhibition of grain growth can be explained by the depressive diffusion process, which reduces GB mobility. Besides, the poor pressing ability of the powders derived from strain hardening during MA leads to an additional processing difficulty in compacting mechanically alloyed powders. The high pressure during consolidation provides a big advantage for producing sufficient plastic deformations of the work-hardened powders, thus effectively fills the space between the powders and densifies the compacts under a relatively low consolidating temperature.

The present study investigates the feasibility of preparing in situ Mg–MgO nanocomposites by reactively cryomilling Mg with oxygen and consolidating the cryomilled powders under a high pressure. MgO is regarded as a good candidate to become a reinforcement in Mg for its excellent mechanical and thermal properties [9, 58, 59]. Meanwhile, the Mg–MgO nanocomposites are cost-effective for practical applications. Our goal is to prepare bulk Mg–MgO nanocomposites with a high content of MgO nanoparticles uniformly distributed in Mg matrix, aimed at achieving Mg–MgO nanocomposites with both high thermal stability and high strength at room and elevated temperatures.

Experimental

The samples were prepared from elemental Mg (Alfa Aesar, 99.9 + %) powders with an average particle size of 80 μm . Two grams of Mg powders and 20 g of hardened steel balls were placed in an argon-filled hardened steel vial. The as-received Mg powders were firstly pre-milled for 5 h at room temperature in a SPEX 8000 M mixer/mill operated inside an argon-filled glove box containing less than 1 ppm oxygen to improve their reactivity during subsequent reactive milling. A few drops of hexane were added to serve as a lubricant to prevent adhering and cold-welding of the ductile Mg powders.

The reactive cryomilling was performed in a sequence of cooling-milling steps. The pre-milled Mg powders were placed in an inflatable hardened steel vial (50 mL). The vial was evacuated and then filled with a gas mixture (50 vol% Ar and 50 vol% O₂) to an internal gas pressure of 1 bar. Subsequently, the vial was immersed in a liquid nitrogen bath for 15 min and then mechanically milled for 15 min. After every two cycles (30 min of cryomilling), the vial was evacuated and then refilled with the gas mixture. Assuming that the reaction between Mg and O was completed after every two cycles; then, a Mg–5vol%MgO composite was achieved. The above procedures were repeated to obtain a series of Mg– x MgO nanocomposites ($x = 5, 10, 20$ and 40 vol%). For comparison, pure Mg firstly pre-milled for 5 h at room temperature and subsequently cryomilled in an Ar atmosphere was also studied.

After the reactive cryomilling, the powders were cold-compacted into rods of 10 mm diameter and 15 mm length inside an argon-filled glove box containing less than 1 ppm oxygen. The compacts were then consolidated by a high-pressure consolidation method at room temperature in a cubic-anvil press (CS-1B). The compacts were wrapped with tantalum foil and then inserted into a BN crucible. A high pressure of 6 GPa was symmetrically loaded. The pressure-holding time was 0.5 h.

The consolidated samples were isochronally annealed for 1 h in an argon-filled glove box containing less than 1 ppm oxygen. The as-cryomilled and the consolidated samples were characterized by X-ray diffraction (XRD), X-ray fluorescence (XRF)

spectroscopy, transmission electron microscopy (TEM), microhardness and compression tests. The XRD was carried out on a D/MAX-2500/PC diffractometer with $\text{CuK}\alpha$ radiation ($\lambda = 0.154 \text{ nm}$) and a graphite monochromator. The peak position and the instrumental broadening were calibrated by using standard Si powders. The average grain sizes and microstrain of the as-cryomilled powders were calculated from X-ray line broadening using the Williamson–Hall method [60]. The volume fraction of the MgO nanophase was analyzed by the Rietveld software. The chemical composition of the samples was analyzed using an ADVANT X'P-381-type X-ray fluorescence spectrometer. Microhardness was measured on the as-cryomilled powders (consolidated at room temperature) with a Vickers hardness tester (FM-ARS-9000) with a load of 50 g and a dwelling time of 15 s. The high-temperature hardness was measured on a Vickers hardness tester (HTV-PHS30) with a load of 200 g and a dwelling time of 10 s. The samples were remained at the testing temperatures for 5 min prior to test. At least ten separate measurements were taken for each sample. After the high-temperature hardness test is completed, the specimen is cooled down to room temperature. Then, the room-temperature hardness is measured. This hardness is called post-testing room-temperature hardness. Compression tests were performed with an INSPEK Table 100 testing machine equipped with a 100-kN load cell at a strain rate of 10^{-3} s^{-1} and at room temperature. The cylindrical compression samples with a diameter of 4 mm and a height of 6 mm were achieved by consolidating the as-cryomilled powders at temperatures between 300 and 600 °C for 0.5 h under a pressure of 6 GPa. The surfaces of all test specimens were polished prior to testing. Teflon sheets were placed between the contacting surfaces for lubrication to avoid barreling. Samples for the transmission electron microscopy (TEM) observation were prepared by twin-jet polishing disks (with a diameter of 3 mm) in a 6 vol% perchloric acid ethanol solution at $-30 \text{ }^\circ\text{C}$. The microstructures were then observed on a JEOL 2010 TEM operated at 200 kV. More than 200 nanograins were counted to obtain an average grain size. In case of AGG, more than 20 micron-sized grains were counted and averaged. On the same TEM machine, high-resolution TEM (HRTEM) images were also recorded to study the microstructures of samples.

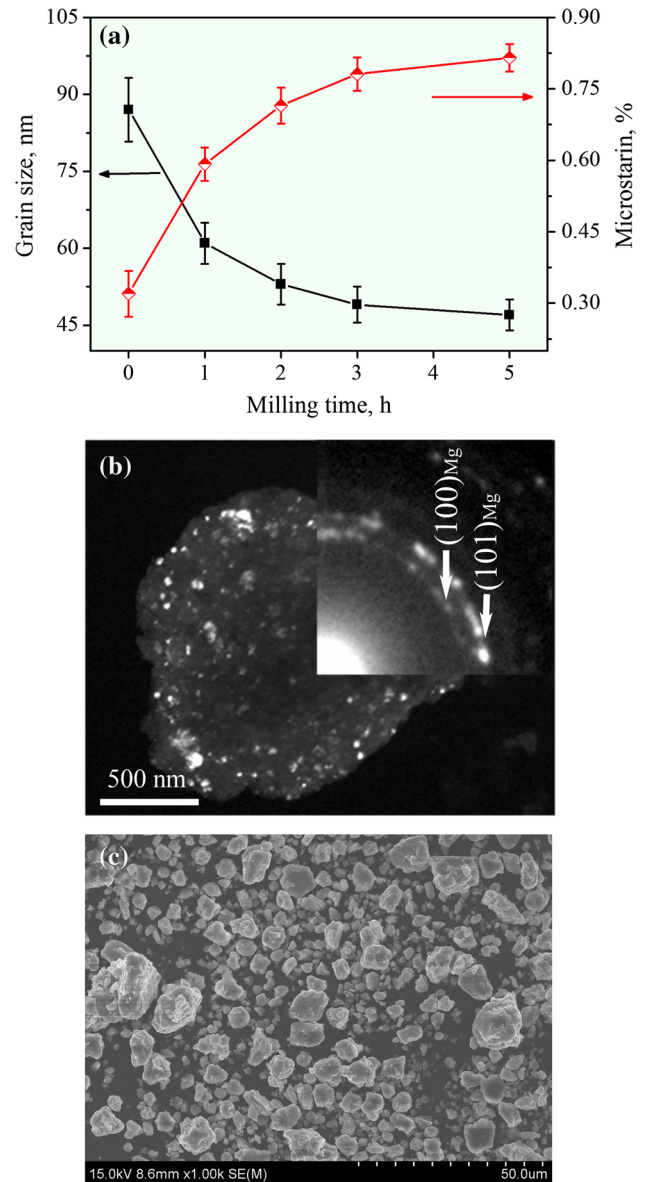


Figure 1 a Grain size and microstrain as a function of cryomilling time for pure Mg. b Dark-field TEM image and the corresponding SEAD pattern of pure Mg powders after 5 h of cryomilling. c SEM image of pure Mg powders after 5 h of cryomilling.

Results and discussion

Microstructures

Figure 1a shows the grain size and microstrain—which are calculated from the X-ray diffraction line broadening data—as a function of cryomilling time for pure Mg. The grain size of starting pure Mg—which was achieved by milling at room temperature for 5 h—is $87 \pm 6.5 \text{ nm}$. The grain size decreases

rapidly to 61 ± 4 nm after 1 h of cryomilling and reaches a stable value of 48 ± 3.2 nm after 5 h of cryomilling. Meanwhile, the microstrain increases rapidly and reaches about 0.78% after 5 h of cryomilling. Figure 1b shows the dark-field TEM image of pure Mg powders after 5 h of cryomilling. The grain size of Mg matrix varies between 25 and 81 nm. The average grain size is 51 ± 4.3 nm, which is consistent with the grain size (48 ± 3.2 nm) calculated from the XRD data. The inset selected-area diffraction (SEAD) pattern shows diffraction rings from 101 and 100 planes of Mg phase. Figure 1c shows the SEM image of pure Mg powders after 5 h of cryomilling. The powders have an average particle size of 8.3 ± 1.7 μm and a faceted shape resulting from repeated fracturing and welding.

Figure 2 shows the XRD patterns of pure Mg and Mg–10MgO. Only diffraction peaks from a hcp Mg phase are observed for pure Mg after 5 h of cryomilling. Nevertheless, a broadening peak around 42.5° corresponding to MgO (200) plane appears for Mg–10MgO after 5 h of cryomilling. The average grain size—calculated from the X-ray diffraction line broadening data—of the Mg and MgO phases in Mg–10MgO is approximately 46 ± 3.7 and 6.8 ± 1.5 nm, respectively. The volume fraction of the MgO nanophas is calculated to be about 8.3%, which is slightly lower than the nominal value (10%). Note that the peaks of the Mg and MgO phases become narrower after thermal annealing.

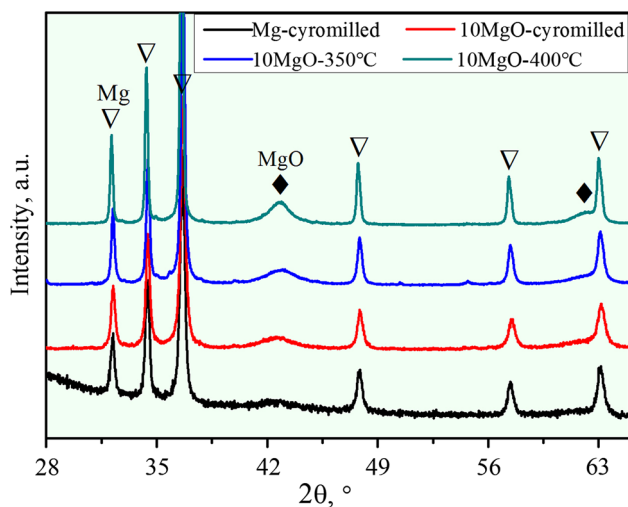


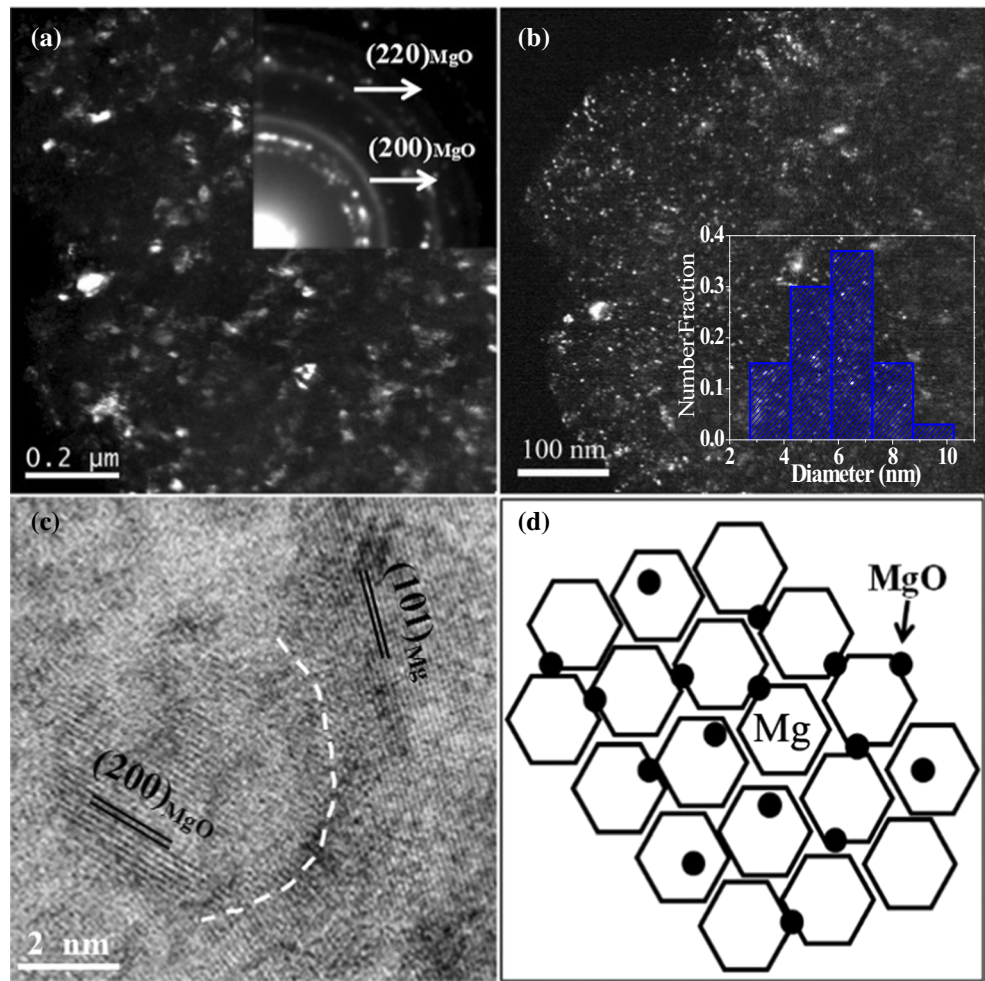
Figure 2 XRD patterns of pure Mg after 5 h of cryomilling and Mg–10MgO after 5 h of cryomilling and subsequently annealing at 350 and 400 °C.

Fig. 3a shows the dark-field TEM image of Mg–10MgO after 5 h of cryomilling. The average grain size of the Mg phase in Mg–10MgO is 49 ± 4.1 nm—which is consistent with the grain size (46 ± 3.7 nm) estimated from the XRD data—and is similar to that of as-cryomilled pure Mg (48 ± 3.2 nm). Note that typical diffraction rings corresponding to MgO (200) and (220) planes are clearly observed in the inset SEAD pattern of Fig. 3a.

The dark-field TEM image obtained using a part of MgO (200) diffraction ring is shown in Fig. 3b. Uniformly distributed MgO nanoparticles with an average particle size of 7.8 ± 1.7 nm can be observed in the Mg matrix. The formation of fine MgO nanoparticles can be attributed to the metastability of high-energy mechanical alloying—a far-from-equilibrium processing method—which is well known for producing supersaturated solid solutions and nanosized dispersions at the finest length scales. Figure 3c shows the HRTEM image of an in situ formed MgO nanoparticle binding with a Mg grain. No debonding or tiny crack can be observed at the interface, revealing a good interfacial integrity between the MgO nanoparticle and the Mg grain. In fact, all of the MgO nanoparticles in our HRTEM images are situated at the GBs of Mg matrix. This can be attributed to the negligible solid solubility of O in Mg. Thus, the in situ reaction between Mg and O atoms mainly occurs at the particle surfaces and GBs. Certainly, the diffusion of O atoms into the Mg lattice during cryomilling may also result in the formation of MgO nanoparticles, which can reside in grain interiors but are with a very limited number density. Figure 3d shows the schematic illustration of MgO nanoparticles mainly residing at GBs.

It is generally assumed that the flaw size in a particle is directly proportional to the particle size [61]. For the present MgO nanoparticles with an average particle size of about 7.8 nm, the flaw size is several orders of magnitude smaller than the conventional micrometer-sized reinforcements. This will result in an extremely high stress to cause the nanoparticles to fracture during deformation. In addition, flaws such as micron-meter scale and nanoscale cracks are more commonly found around the larger reinforced particles. This will inevitably lead to interfacial failures [62]. In contrast, nanoparticles reinforced composites are less likely to fail by interfacial decohesion due to their good particle/matrix interfacial bonding. Furthermore, our

Figure 3 **a** Dark-field TEM image and the corresponding SEAD pattern of Mg–10MgO after 5 h of cryomilling. **b** Dark-field TEM image obtained using a part of the (200) MgO diffraction ring. Inset shows the size distribution of MgO nanoparticles. **c** HRTEM image of an in situ formed MgO nanoparticle binding with a Mg grain. **d** Schematic illustration of the distribution of MgO nanoparticles at GBs and in grain interiors.



in situ reaction process results in the nanocomposites with a clean MgO particle/Mg matrix interface. All of the above factors help improve the thermal stabilities and mechanical behaviors of Mg–MgO nanocomposites.

Thermal stability

Figure 4 shows the TEM images of nanocrystalline Mg and Mg–10MgO nanocomposites annealed for 1 h. A bimodal microstructure occurs in nanocrystalline Mg annealed at 200 °C, where isolated large micron-sized grains due to an AGG coexist with ultrafine-grained (275 nm) matrix, as shown in Fig. 4a. Large grains without any residual nanometer-sized grains are observed throughout the sample annealed at 300 °C (Fig. 4b). In contrast, the average grain size of Mg–10MgO annealed at 350 °C slightly increases to 108 ± 33 nm, as shown in Fig. 4c, indicative of a high thermal stability of Mg

nanograins. In addition, the particle size of MgO nanoparticles slightly increases from 7.8 ± 1.7 nm to 9.3 ± 3.7 nm (Fig. 4d), indicative of a high thermal stability of MgO nanoparticles. Annealing at 400 °C causes the entire microstructure of Mg–10MgO to grow to 182 ± 62 nm, as shown in Fig. 4e. It is noteworthy that some clusters of MgO nanoparticles occur, as indicated by the white arrows in Fig. 4f. In addition, the average particle size of MgO nanoparticles increases from 9.3 ± 3.7 nm to 15.3 ± 4.5 nm.

Figure 5 shows the grain size versus annealing temperature for nanocrystalline Mg and Mg–10MgO nanocomposite. Initial grain size of the two samples is ~ 50 nm. However, a rapid grain growth occurs at ~ 100 °C ($0.40 T_m$, where T_m is the melting point of pure Mg) and ~ 400 °C ($0.73 T_m$) for nanocrystalline Mg and Mg–10MgO, respectively. This clearly indicates that Mg–10MgO nanocomposite has a much higher thermal stability. At 400 °C, the average grain size of pure Mg reaches 17.5 ± 5.2 μm , whereas that

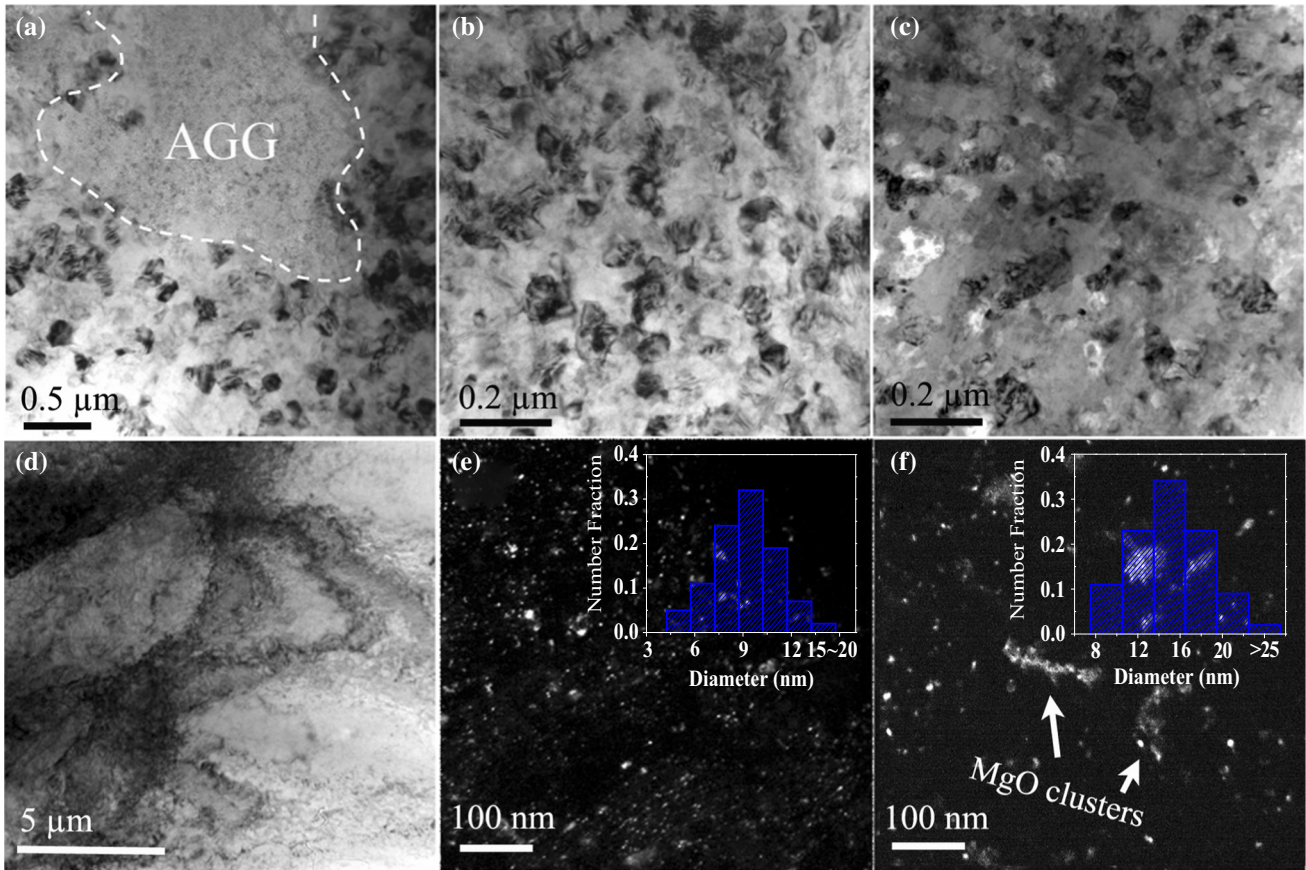


Figure 4 Bright-field TEM images of nanocrystalline Mg annealed at **a** 200 °C and **b** 300 °C for 1 h. **c** Bright-field TEM image of Mg–10MgO nanocomposite annealed at 350 °C for 1 h and **d** the corresponding dark-field image obtained from the MgO

(200) plane. **e** Bright-field TEM image of Mg–10MgO nanocomposite annealed at 400 °C for 1 h and **f** the corresponding dark-field image obtained from the MgO (200) plane. Insets in **e** and **f** show the size distribution of MgO nanoparticles.

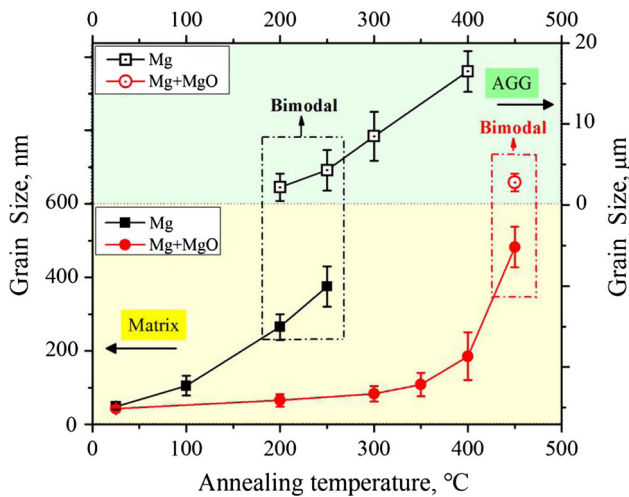


Figure 5 Grain size of nanocrystalline Mg and Mg–10MgO nanocomposite as a function of annealing temperature.

of Mg–10MgO is still as small as 182 ± 62 nm. However, annealing at 450 °C leads to an AGG for

Mg–10MgO. This AGG can be attributed to the localized inhomogeneous distribution of MgO nanoparticles due to their aggregations during annealing.

The high thermal stability of Mg–10MgO can be ascribed to the kinetic stabilization mechanism, i.e., the Zener pinning [63], where normal grain growth would be completely inhibited by second-phase particles. The grain size predicted by Zener is given by the equation, $d = 4r/3f_v$, where d is the grain size of the matrix, r is the particle size of the secondary particles, and f_v is the volume fraction of the particles. It is clear that a high volume fraction of secondary particles with a small particle size is desirable to effectively impede GB mobility and stabilize the matrix at a small grain size. Using our experimentally measured average r of 9.3 ± 3.7 and 15.3 ± 4.5 nm and f_v of 8.3%, one obtains a stabilized d of 149 ± 59 and 246 ± 72 nm for Mg–10MgO annealed at 350 and

Table 1 Chemical composition (wt%) of the raw and as-milled Mg powders

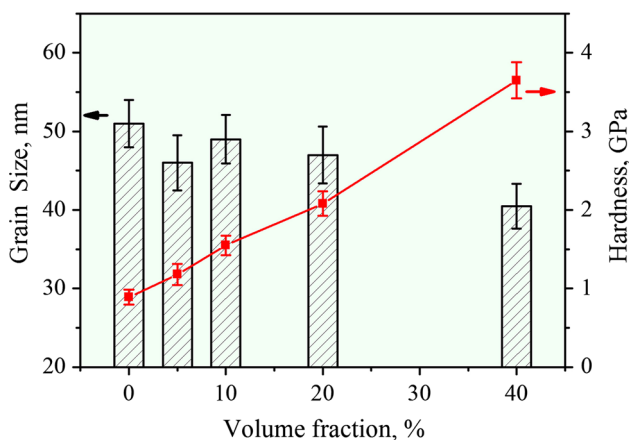
Elements	Zn	Fe	C	O	Cr
Raw	0.0075	0.0083	0.004	0.025	
As-milled	0.0063	0.0165	0.0049	0.042	0.0033

400 °C, respectively. These calculated values agree well with the grain sizes (108 ± 33 and 182 ± 62 nm) obtained by TEM observations.

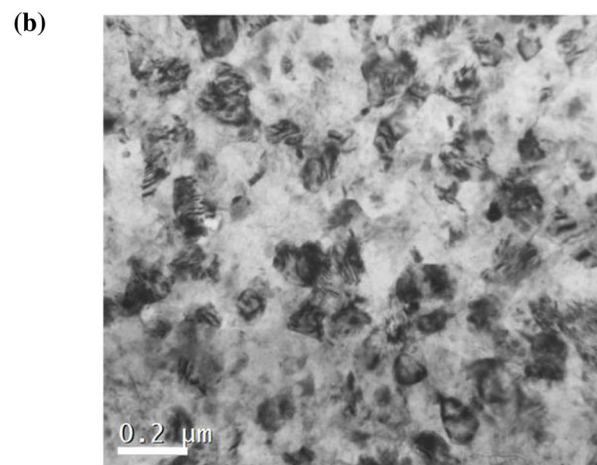
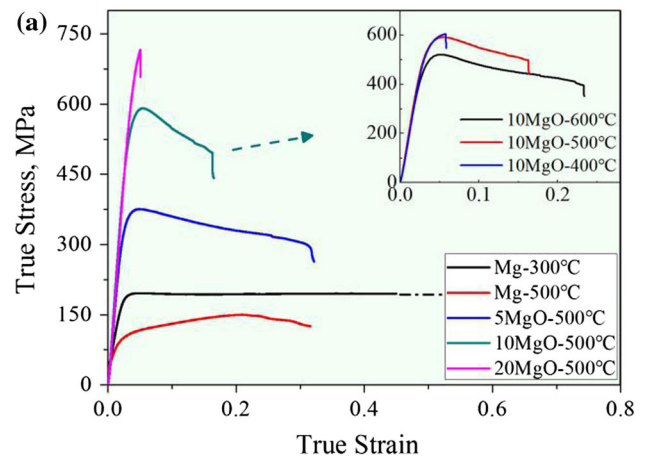
Note that MA inevitably introduces such impurities as Fe that may kinetically pin the grains. Table 1 shows the chemical analysis results of the raw and as-milled Mg powders. It can be seen that the content of impurities, such as Fe and Cr, is relatively low after mechanical alloying. Thus, the pinning effect caused by impurities is negligible. Our experimental results suggest that the kinetic stabilization by the MgO nanoparticles mainly residing at GBs should be the dominant factor for the observed high thermal stability of Mg–10MgO nanocomposites. This is because the content of impurities in nanocrystalline Mg should be similar to that in Mg–10MgO nanocomposites. However, the former has a thermal stability much lower than the latter.

Mechanical properties

Figure 6 shows the dependence of grain size and microhardness of cryomilled Mg– x MgO powder compacts on the volume fraction of MgO nanoparticles. The powder compacts were made by

**Figure 6** Dependence of grain size and microhardness of cryomilled Mg– x MgO ($x = 0$ –40 vol%) powder compacts on the volume fraction of MgO nanoparticles.

consolidating the as-cryomilled powders at room temperature. It is interesting to note that the initial average grain sizes of all samples (except for Mg–40MgO) are approximately 50 nm, suggesting that the influence of the volume fraction of MgO nanoparticles on the grain size of Mg matrix is negligible. This is understandable since MgO nanoparticles are mainly situated at the GBs of Mg matrix and do not essentially alter the dislocation storage capacities in grain interiors. However, the average grain size of Mg–40MgO is about 41 nm, suggesting that the number of MgO nanoparticles residing in grain interiors of this sample should be sufficient to further refine the grain size of Mg matrix. Meanwhile, the hardness of powder compacts increases almost linearly with the content of MgO nanoparticles. As a

**Figure 7** **a** Room-temperature compressive stress–strain curve of cryomilled Mg and Mg– x MgO after a high-pressure (6 GPa) consolidation at different temperatures. Inset shows the stress–strain curve of Mg–10MgO consolidated under 6 GPa at different temperatures. **b** Bright-field TEM image of Mg–10MgO consolidated under 6 GPa at 500 °C for 0.5 h.

result, a high hardness value of 3.65 GPa is obtained for Mg–40MgO powder compact.

Figure 7a shows the room-temperature stress–strain curve of the consolidated bulk Mg and Mg–*x*MgO nanocomposites. The corresponding compressive mechanical properties are summarized in Table 2. The yield strength of Mg–*x*MgO nanocomposites increases with the content of MgO nanoparticles. Nanocrystalline Mg obtained by consolidating the cryomilled pure Mg powders under a high pressure of 6 GPa at 300 °C (Mg-300 °C) has a relatively high yield strength of 179 MPa and a large fracture strain (> 0.8 true strain) with no strain hardening. Our TEM observation (not shown here) indicates that the Mg-300 °C sample maintains a fine microstructure with an average grain size of 132 ± 63 nm. However, the average grain size of as-cryomilled nanocrystalline Mg increases to 8.4 ± 5.3 μm after annealing under atmospheric pressure at 300 °C. Thus, the fine grain size of Mg-300 °C sample can be attributed to the depressive effect of high pressure on the grain growth. Consolidating the Mg powders under 6 GPa at 500 °C, however, results in a micrometer-scale Mg bulk with a low strength of 73 MPa. In contrast, high yield strengths of 355 and 562 MPa are achieved for Mg–5MgO and Mg–10MgO, respectively, after consolidation under 6 GPa at 500 °C. Moreover, a higher yield strength of 688 MPa is obtained for Mg–20MgO. However, the Mg–20MgO sample has negligible fracture strain. The achieved high strength can be mainly attributed to two factors: (1) the fine microstructures, as shown in Fig. 7b, which can be ascribed to the kinetic pinning effects by the MgO nanoparticles combined with depressive effect of high pressure on the grain growth. (2) The strong atomic interfacial bonding, which can effectively transfer the mechanical load from the Mg matrix to the MgO nanoparticles.

Table 2 Yield strength, ultimate strength and fracture strain of bulk Mg and Mg–*x*MgO after consolidating under 6 GPa at different temperatures

Sample	Yield strength (MPa)	Ultimate strength (MPa)	Fracture strain (%)
Mg-300 °C	179	193	> 80
Mg-500 °C	73	152	31.8
Mg–5MgO-500 °C	355	378	32.6
Mg–10MgO-400 °C	575	603	5.9
Mg–10MgO-500 °C	562	592	16.3
Mg–10MgO-600 °C	482	528	23.4
Mg–20MgO-500 °C	688	718	5.6

The inset in Fig. 7a shows the stress–strain curve of Mg–10MgO consolidated under 6 GPa at different temperatures. The Mg–10MgO sample consolidated at 400 °C exhibits a high yield strength of 575 MPa but fractures in the early stage of the compressive deformation. The Mg–10MgO consolidated at 500 °C has both a high strength of 562 MPa and a larger fracture strain of 16.3%. The high thermal stability of Mg–10MgO nanocomposites enables us to consolidate the as-cryomilled composite powders at a high temperature—where a better interfacial bonding between powder particles can be achieved—with the retaining of their fine microstructures.

The hardness and strength of particle-reinforced metal matrix composites are often saturated when the content of the particles increases [9–11, 27, 64]. This is mainly attributed to the difficulties in uniformly dispersing the nanoparticles with a high content and the tendency to form particle/matrix interfacial cracks upon deforming. For example, the strength of Mg–TiC nanocomposites synthesized by in situ mechanical alloying is saturated at ~ 300 MPa when the volume fraction of TiC nanoparticles is above 15% [27]. The in situ formed TiC nanoparticles are mechanically mixed with the Mg matrix without a strong interfacial bonding. It is expected that these TiC nanoparticles can be transported or moved with GB sliding during deformation, resulting in a relatively low saturation value of flow stress [27]. In contrast, the present MgO nanoparticles are synthesized by the in situ reaction between the Mg matrix and O atoms during cryomilling. The in situ process results in clean interfaces between the MgO nanoparticles and Mg matrix with a good interfacial integrity. These interfaces can act as obstacles to GB mediated deformation and thus effectively increase the flow stress. As expected, the hardness (shown in Fig. 6) and strength (shown in Fig. 7) of our in situ Mg–MgO nanocomposites increase linearly with the content of MgO nanoparticles.

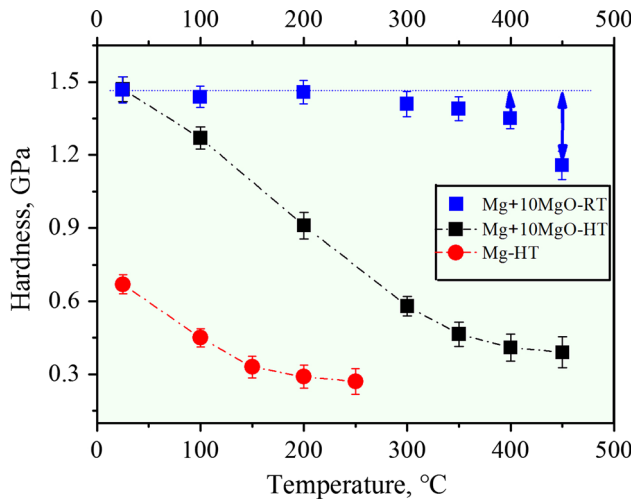


Figure 8 High-temperature (HT) hardness of pure Mg (consolidated at 300 °C) and Mg–10MgO (consolidated at 500 °C) versus testing temperature. Also shown is the post-testing room-temperature (RT) hardness of Mg–10MgO after high-temperature hardness testing at various temperatures.

The effect of temperature on the hardness is illustrated in Fig. 8. The high-temperature hardness decreases linearly and reaches a stable value of ~ 0.3 GPa at ~ 200 °C for nanocrystalline Mg and 0.4 GPa at ~ 400 °C for Mg–10MgO, respectively. Note that no significant change in the post-testing room-temperature hardness of Mg–10MgO is observed when the temperature for the high-temperature hardness test is below 400 °C. This can be mainly attributed to the high thermal stability, i.e., the retaining of the fine microstructure. Another noteworthy part of Mg–10MgO is the higher high-temperature hardness when compared with pure Mg. For nanocrystalline materials, grain-boundary activities such as grain-boundary sliding have been proposed for their plastic deformations at elevated temperatures [53, 65]. Thus, it is possible that the in situ formed MgO nanoparticles—which have a strong atomic bonding with the Mg grains—should pin the GBs and increase the barrier strength for such grain-boundary activities at elevated temperatures.

Conclusions

The Mg–MgO in situ nanocomposites are successfully synthesized by reactively cryomilling Mg with oxygen and subsequently consolidating the cryomilled powders under a high pressure of 6 GPa. The

microstructures, thermal stabilities and mechanical behaviors of the Mg–MgO nanocomposites are investigated and summarized as below:

1. A uniform distribution of MgO nanoparticles with an average particle size of 7.8 ± 1.7 nm is achieved in Mg–MgO nanocomposite by reactively cryomilling Mg powders with oxygen. The MgO nanoparticles are mainly situated at the GBs of Mg matrix and have a strong interfacial bonding with the Mg matrix.
2. When compared with nanocrystalline Mg, the thermal stability of Mg–10MgO nanocomposite is largely enhanced. A rapid grain growth is observed at ~ 100 °C ($0.4 T_m$) and 400 °C ($0.73 T_m$) for nanocrystalline Mg to 450 °C for Mg–10MgO. The high thermal stability of Mg–10MgO is mainly ascribed to the kinetic stabilization mechanism, i.e., the Zener pinning effect of the in situ formed MgO nanoparticles located at GBs.
3. The hardness of Mg–MgO nanocomposites increases almost linearly with the content of MgO nanoparticles and reaches 3.65 GPa for Mg–40vol%MgO. Moreover, the high thermal stability of Mg–10MgO nanocomposite enables us to consolidate the cryomilled powders under 6 GPa at a high temperature of 500 °C and achieve a bulk Mg–10MgO nanocomposite with a high compressive yield strength of 562 MPa and a relatively large fracture strain of 16.3%. The yield strength of Mg–20MgO can be as high as 688 MPa. However, this nanocomposite has negligible fracture strain.
4. The in situ formed MgO nanoparticles with a strong atomic bonding with the Mg grains can pin the grain-boundary activities and thus significantly improve the high-temperature hardness below 400 °C.

Acknowledgements

This work was financially supported by the National Natural Science Foundation of China (Grant Number 11575154) and the High-Level Talents Research Program of the Yanshan University (Grant Number 005000201).

References

- [1] Kim CS, Sohn I, Nezafati M et al (2013) Prediction models for the yield strength of particle-reinforced unimodal pure magnesium (Mg) metal matrix nanocomposites (MMNCs). *J Mater Sci* 48:4191–4204. <https://doi.org/10.1007/s10853-013-7232-x>
- [2] Shen MJ, Wang XJ, Li CD et al (2014) Effect of submicron size SiC particles on microstructure and mechanical properties of AZ31B magnesium matrix composites. *Mater Des* 54:436–442
- [3] Nie KB, Deng KK, Xu FJ, Wang XJ, Wu K (2015) Development of microstructure in submicron particles reinforced magnesium matrix composite processed by room temperature deformation. *Mater Chem Phys* 149:21–26
- [4] Wang XJ, Wang NZ, Wang LY et al (2014) Processing, microstructure and mechanical properties of micro-SiC particles reinforced magnesium matrix composites fabricated by stir casting assisted by ultrasonic treatment processing. *Mater Des* 57:638–645
- [5] Chen LY, Xu JQ, Choi H et al (2015) Processing and properties of magnesium containing a dense uniform dispersion of nanoparticles. *Nature* 528:539–543
- [6] Ma X, Zhao YF, Tian WJ et al (2016) A novel Al matrix composite reinforced by nano-AlNp network. *Sci Rep* 6:34919–34927
- [7] Kim CS, Cho K, Manjili MH, Nezafati M (2017) Mechanical performance of particulate-reinforced Al metal-matrix composites (MMCs) and Al metal-matrix nano-composites (MMNCs). *J Mater Sci* 52:13319–13349. <https://doi.org/10.1007/s10853-017-1378-x>
- [8] Bagherpour E, Reihanian M, Miyamoto H (2017) Tailoring particle distribution non-uniformity and grain refinement in nanostructured metal matrix composites fabricated by severe plastic deformation (SPD): a correlation with flow stress. *J Mater Sci* 52:3436–3446. <https://doi.org/10.1007/s10853-016-0632-y>
- [9] Goh CS, Gupta M, Wei J, Lee LC (2007) Characterization of high performance Mg/MgO nanocomposites. *J Compos Mater* 41:2325–2335
- [10] Tjong SC (2007) Novel nanoparticle-reinforced metal matrix composites with enhanced mechanical properties. *Adv Eng Mater* 9:639–652
- [11] Ferguson JB, Sheykh-Jaberi F, Kim CS, Rohatgi PK, Cho K (2012) On the strength and strain to failure in particle-reinforced magnesium metal-matrix nanocomposites (Mg MMNCs). *Mater Sci Eng A* 558:193–204
- [12] Chen LY, Konishi H, Fehrenbacher A et al (2012) Novel nanoprocessing route for bulk graphene nanoplatelets reinforced metal matrix nanocomposites. *Scr Mater* 67:29–32
- [13] Tan XH, Chee WKH, Chan JKW, Kwok RWO, Gupta M (2016) Stretching the engineering strain of high strength LPSO quaternary Mg–Y–Zn–Al alloy via integration of nano-Al₂O₃. *J Mater Sci* 51:4160–4168. <https://doi.org/10.1007/s10853-016-9742-9>
- [14] Donnadiou P, Benrhaiem S, Tassin C, Volpi F, Blandin JJ (2017) Preparation, microstructure and properties of magnesium- γ Mg₁₇Al₁₂ complex metallic alloy in situ composites. *J Alloys Compd* 702:626–635
- [15] Ghasali E, Alizadeh M, Niazmand M, Ebadzadeh T (2017) Fabrication of magnesium-boron carbide metal matrix composite by powder metallurgy route: comparison between microwave and spark plasma sintering. *J Alloys Compd* 697:200–207. <https://doi.org/10.1016/j.jallcom.2016.12.146>
- [16] Paramsothy M, Gupta M (2013) ZrB₂ nanoparticle induced nano-LPSO-grain and nano-LPSO-layer reinforced ultra-high strength Mg–RE alloy. *J Mater Sci* 48:8368–8376. <https://doi.org/10.1007/s10853-013-7647-4>
- [17] Song K, Zhang J, Liu L (2014) An Al₂O₃/Y₃Al₅O₁₂ eutectic nanocomposite rapidly solidified by a new method: liquid–metal quenching. *Scr Mater* 92:39–42
- [18] Chen J, Bao CG, Ma YN, Chen ZH (2017) Distribution control of AlN particles in Mg–Al/AlN composites. *J Alloys Compd* 695:162–170
- [19] Cai XC, Song J, Yang TT, Peng QM, Huang JY, Shen TD (2018) A bulk nanocrystalline Mg–Ti alloy with high thermal stability and strength. *Mater Lett* 210:121–123
- [20] Lü L, Lai MO, Liang W (2004) Magnesium nanocomposite via mechanochemical milling. *Compos Sci Technol* 64:2009–2014
- [21] Lü L, Lai MO, Toh YH, Froyen L (2002) Structure and properties of Mg–Al–Ti–B alloys synthesized via mechanical alloying. *Mater Sci Eng A* 334:163–172
- [22] Ferkel H, Mordike BL (2001) Magnesium strengthened by SiC nanoparticles. *Mater Sci Eng A* 298:193–199
- [23] Garroni S, Delogu F, Minella CB, Pistidda C, Cuesta-Lopez S (2017) Mechanically activated metathesis reaction in NaNH₂–MgH₂ powder mixtures. *J Mater Sci* 52:11891–11899. <https://doi.org/10.1007/s10853-017-1220-5>
- [24] Wang FL, Li YP, Wang XY, Koizumi Y, Kenta Y, Chiba A (2016) In-situ fabrication and characterization of ultrafine structured Cu–TiC composites with high strength and high conductivity by mechanical milling. *J Alloys Compd* 657:122–132
- [25] Zhang F, Kaczmarek WA, Lü L, Lai MO (2000) Formation of titanium nitrides via wet reaction ball milling. *J Alloys Compd* 307:249–253
- [26] Blázquez JS, Ipus JJ, Moreno-Ramírez LM et al (2017) Ball milling as a way to produce magnetic and magnetocaloric

- materials: a review. *J Mater Sci* 52:11834–11850. <https://doi.org/10.1007/s10853-017-1089-3>
- [27] Hwang S, Nishimura C, McCormick P (2001) Compressive mechanical properties of Mg–Ti–C nanocomposite synthesized by mechanical milling. *Scr Mater* 44:2457–2462
- [28] Tjong SC, Ma ZY (2000) Microstructural and mechanical characteristics of in situ metal matrix composites. *Mater Sci Eng R* 29:49–113
- [29] Yang CL, Zhang B, Zhao DC et al (2017) In-situ synthesis of AlN/Mg–Al composites with high strength and high plasticity. *J Alloys Compd* 699:627–632
- [30] Gangil N, Siddiquee AN, Maheshwari S (2017) Aluminium based in situ composite fabrication through friction stir processing: a review. *J Alloys Compd* 715:91–104
- [31] Wang XM, Jha A, Brydson R (2004) In situ fabrication of Al₃Ti particle reinforced aluminium alloy metal-matrix composites. *Mater Sci Eng A* 364:339–345
- [32] Wang XM, Jha A, Brydson R, Ellis J (1999) Microstructural analysis of Al alloys dispersed with TiB₂ particulate for MMC applications. *J Microsc* 196:137–145
- [33] Chen C, Cui CX, Zhao LC, Liu SQ, Liu SJ (2016) The formation mechanism and interface structure characterization of in situ AlN/Al composites. *J Compos Mater* 50:495–506
- [34] Glagea A, Ceccatob R, Lonardelli I et al (2009) A powder metallurgy approach for the production of a MgH₂–Al composite material. *J Alloys Compd* 478:273–280
- [35] Yang N, Yee JK, Zhang ZH et al (2015) Hydrogen sorption characteristics of nanostructured Pd–10Rh processed by cryomilling. *Acta Mater* 82:41–50
- [36] Witkin DB, Lavernia EJ (2006) Synthesis and mechanical behavior of nanostructured materials via cryomilling. *Prog Mater Sci* 51:1–60
- [37] Saller BD, Hu T, Ma K et al (2015) A comparative analysis of solubility, segregation, and phase formation in atomized and cryomilled Al–Fe alloy powders. *J Mater Sci* 50:4683–4697. <https://doi.org/10.1007/s10853-015-9019-8>
- [38] Abdu MT, Dheda SS, Lavernia EJ et al (2013) Creep and microstructure in ultrafine-grained 5083 Al. *J Mater Sci* 48:3294–3303. <https://doi.org/10.1007/s10853-012-7115-6>
- [39] Lavernia EJ, Han BQ, Schoenung JM (2008) Cryomilled nanostructured materials: processing and properties. *Mater Sci Eng A* 493:207–214
- [40] Birringer R (1989) Nanocrystalline materials. *Mater Sci Eng A* 117:33–43
- [41] Cao P, Lu L, Lai MO (2001) Grain growth and kinetics for nanocrystalline magnesium alloy produced by mechanical alloying. *Mater Res Bull* 36:981–988
- [42] Thein MA, Lu L, Lai MO (2006) Kinetics of grain growth in nanocrystalline magnesium-based metal-metal composite synthesized by mechanical alloying. *Compos Sci Technol* 66:531–537
- [43] Chen Z, Liu F, Wang HF et al (2009) A thermokinetic description for grain growth in nanocrystalline materials. *Acta Mater* 57:1466–1475
- [44] Darling KA, Tschopp MA, VanLeeuwen BK, Atwater MA, Liu ZK (2014) Mitigating grain growth in binary nanocrystalline alloys through solute selection based on thermodynamic stability maps. *Comput Mater Sci* 84:255–266
- [45] Chookajorn T, Murdoch HA, Schuh CA (2012) Design of stable nanocrystalline alloys. *Science* 337:951–954
- [46] Darling KA, VanLeeuwen BK, Semones JE (2011) Stabilized nanocrystalline iron-based alloys: guiding efforts in alloy selection. *Mater Sci Eng A* 528:4365–4371
- [47] Saber M, Kotan H, Koch CC, Scattergood RO (2013) A predictive model for thermodynamic stability of grain size in nanocrystalline ternary alloys. *J Appl Phys* 114(10):103510
- [48] Kotan H, Darling KA, Saber M, Scattergood RO, Koch CC (2013) An in situ experimental study of grain growth in a nanocrystalline Fe₉₁Ni₈Zr₁ alloy. *J Mater Sci* 48:2251–2257. <https://doi.org/10.1007/s10853-012-7002-1>
- [49] Saber M, Kotan H, Koch CC, Scattergood RO (2012) Thermal stability of nanocrystalline Fe–Cr alloys with Zr additions. *Mater Sci Eng A* 556:664–670
- [50] Koch CC, Scattergood RO, Saber M, Kotan H (2013) High temperature stabilization of nanocrystalline grain size: thermodynamic versus kinetic strategies. *J Mater Sci* 28:1785–1791. <https://doi.org/10.1557/jmr.2012.429>
- [51] Kotan H, Darling KA, Scattergood RO, Koch CC (2014) Influence of Zr and nano-Y₂O₃ additions on thermal stability and improved hardness in mechanically alloyed Fe base ferritic alloys. *J Alloys Compd* 615:1013–1018
- [52] Boylan K, Ostrander D, Erb U, Palumbo G, Aust KT (1991) An in situ tem study of the thermal stability of nanocrystalline NiP. *Scr Mater* 25:2711–2716
- [53] Darling KA, Rajagopalan M, Komarasamy M, Bhatia MA, Hornbuckle BC, Mishra RS, Solanki KN (2016) Extreme creep resistance in a microstructurally stable nanocrystalline alloy. *Nature* 537:378–381
- [54] Krasnowski M, Kulik T (2007) Nanocrystalline FeAl matrix composites reinforced with TiC obtained by hot-pressing consolidation of mechanically alloyed powders. *Intermetallics* 15:1377–1383
- [55] Krasnowski M, Kulik T (2010) Nanocrystalline Al–Fe intermetallics-light weight alloys with high hardness. *Intermetallics* 18:47–50
- [56] Cai XC, Yang TT, Yu H, Sun BR, Peng QM, Shen TD (2017) A thermally stable and strong Mg–MgF₂ nanocomposite. *Mater Lett* 209:476–478

- [57] Shewmon PG (1963) Diffusion in solids. McGraw-Hill, New York
- [58] Yuan QH, Zeng XH, Liu Y (2016) Microstructure and mechanical properties of AZ91 alloy reinforced by carbon nanotubes coated with MgO. *Carbon* 96:843–855
- [59] Chaubey AK, Scudino S, Khoshkhoo MS (2014) High-strength ultrafine grain Mg–7.4%Al alloy synthesized by consolidation of mechanically alloyed powders. *J Alloys Compd* 610:456–461
- [60] Ungár T, Révész Á, Borbély A (1998) Dislocations and grain size in electrodeposited nanocrystalline Ni determined by the modified Williamson–Hall and Warren–Averbach procedures. *J Appl Cryst* 31:554–558
- [61] Seshan S, Jayamathy M, Kailas SV, Srivatsan TS (2003) The tensile behavior of two magnesium alloys reinforced with silicon carbide particulates. *Mater Sci Eng A* 363:345–351
- [62] Lloyd DJ (1994) Particle reinforced aluminium and magnesium matrix composites. *Int Mater Rev* 39:1–23
- [63] Humphreys FJ, Hatherly M (1996) Recrystallization and related annealing phenomena. Elsevier Science Inc, New York
- [64] Rawer JC, Krabbe RA, Wittenberger JD (1997) Hot-extrusion of attrition milled iron alloy powders. *Scr Mater* 37:2053–2059
- [65] Hwang S, Nishimura C, McCormick PG (2001) Deformation mechanism of nanocrystalline magnesium in compression. *Scr Mater* 44:1507–1511